16th Australasian Fluid Mechanics Conference
Crown Plaza, Gold Coast, Australia
2-7 December 2007

Particle Image Velocimetry Measurements over an Aerodynamically Open Two-Dimensional Cavity

P. Manovski[1], M. Giacobello[1] and J. Soria[2]

[1]Air Vehicles Division, Defence Science & Technology Organisation,
Melbourne, Victoria, 3207 AUSTRALIA

[2]Laboratory for Turbulence Research in Aerospace & Combustion, Department of Mechanical Engineering
Monash University, Melbourne, Victoria, 3800 AUSTRALIA

Abstract

An experimental study has been undertaken to characterise the low Reynolds number flow over an aerodynamically open two-dimensional cavity of rectangular cross-section. A series of water tunnel experiments have been performed in which the flow field was initially examined using dye flow visualisation, then particle image velocimetry (PIV) was used to obtain quantitative velocity measurements. For a laminar upstream boundary layer, the cavity flow structure has been characterised for a cavity length-to-depth ratio of 5 and Reynolds numbers, based on cavity depth, of 990, 1930, 3780 and 5710. Three different flow regimes were identified over the Reynolds number range tested. The mean PIV flow fields are presented and are found to compare well with the flow visualisation study and existing PIV literature.

Introduction

The flow over cavities is of interest in a range of application where cut-outs exist. These include air-vehicle internal weapon bays, cut-outs on automobiles components and on underwater vehicles. Recent studies have focused on moderate to high Mach numbers and Reynolds numbers, with only a small number of investigations dealing with incompressible flows at relatively low Reynolds numbers. The aim of the present study is to characterise the low Reynolds number laminar flow over a two-dimensional rectangular cross-section cavity using both qualitative and quantitative methods.

Cavity flows remain of interest due to the presence of self-sustained oscillations of the cavity shear layer between the freestream flow and fluid in the cavity. These oscillations can cause acoustic waves (noise), increased drag and structural vibrations. Rossiter [1] is credited as the first to describe the complex feedback process evident in cavity flows. It begins with the formation of an unsteady shear layer from the upstream edge of the cavity, within which discrete vortices are formed. These vortices interact with the downstream edge of the cavity and a pressure disturbance is generated. The acoustic waves propagate upstream, and excite further disturbances in the shear layer, creating a feedback loop, which can lead to self-sustained oscillations at discrete resonant frequencies. For incompressible flows a similar mechanism exists, but instead of producing acoustic waves, vortical disturbances moving past the downstream edge produce an irrotational field which excites further shear layer disturbances.

The length-to-depth ratio (L/D) has been shown to be a dominant parameter in characterising the type of flow field in the cavity. Cavity flow can be either defined as 'open' or 'closed'. A cavity is open if the shear layer reattaches at the trailing edge of the cavity, and closed if the shear layer reattaches on the cavity floor and separates again to reattach at the trailing edge. Experimental studies Sarohia [2] at low speeds (with laminar upstream conditions) typically show that cavities are open for $L/D < 7$ and closed for $L/D > 8$, with a transitional flow occurring in between. Other studies, such as Grace *et al.* [3] have shown that the differentiation point between open and closed cavities may vary slightly depending on the freestream velocity of the flow.

Neary [4] investigated the shear layer oscillations in a two-dimensional rectangular cavity placed in a water tunnel for several low Reynolds numbers, by simultaneous pressure measurements and dye flow visualisation. Three different types of unstable shear layer behaviour were observed. The first occurred at a Reynolds number based on cavity depth, Re_D, of 2450 and was characterised by a small amplitude modulation. The second occurred at $Re_D = 2500$, where the oscillations were characterised by larger amplitudes and an increased amplitude modulation. The third occurred at $Re_D = 2620$, where the shear layer exhibited periods of regular and irregular behaviour with the irregular oscillations occurring more frequently and with greater intensity.

The unsteady flow structure due to a turbulent boundary layer past a rectangular 2D cavity was characterised by Rockwell and Lin [5] using PIV in a large open water tunnel for $Re_D = 27000$. Patterns of organised small- and large-scale vortical structures were observed. The large-scale vortices induced ordered pressure fluctuations, and their magnitude and phase shift were determined using simultaneous imaging and pressure measurements. Within the cavity, a jet-like flow occurred along the cavity floor, which was found to modulate the separated shear layer at the leading edge of the cavity. The time-averaged vorticity and Reynolds stress plots revealed that the turbulence in the separated shear layer along the mouth of the cavity and in the jet-like flow within the cavity rapidly dominates the turbulent structure of the inflow.

A PIV study of a laminar, open cavity flow in a subsonic wind tunnel was performed by Özsoy *et al.* [6]. Significant variations of flow structure, exhibiting primary and secondary cavity vortices were observed at $Re_D = 4000$, 9000 and 13000. The size and distribution of vortices within the cavity changed with Reynolds number. Furthermore, the distribution of turbulent stresses and the number of vortical structures detected was also dependent on Reynolds number.

A recent PIV study was performed by Ashcroft and Zhang [7] on a turbulent, open cavity flow for $Re_D \sim 10^5$. The shear layer growth with respect to downstream distance was found to be independent of the L/D tested (2, 3 and 4) and the range of Reynolds numbers tested. Increasing the length of the cavity allowed a greater period of growth of the vortical structures within the shear layer before impinging upon the trailing face of the cavity. The evolution of the vortical structures was found to be analogous to that of a free shear layer.

The available experimental data on cavity flows consists principally of point-wise instantaneous measurements of velocity, and mean flow field measurements of pressure and/or velocity, as well as qualitative flow visualisation using dye or smoke. Unlike point-wise measurements PIV can yield whole field quantitative measurements of the complex instantaneous and mean velocity flow fields, revealing patterns of velocity, vorticity and streamline topology. However, only a limited number of cavity flow PIV experiments have been carried out, but in contrast to the present study, these have mostly involved turbulent inflows at relatively high Reynolds numbers.

Test Facility & Model Configuration

The water tunnel at DSTO Melbourne is an Eidetics Model 1520H and it has a horizontal-flow test section 380 mm wide, 510 mm deep and 1630 mm long. It is a recirculating closed-circuit tunnel with a free water surface. The side walls and floor of the test section are made from glass to facilitate flow visualisation studies. The freestream velocity (U_∞) in the test section can be varied between 0 and 0.6 m/s, with a variation of less than ± 2% relative to the average value, the mean flow angularity is less than ± 1°, and the turbulence intensity is less than 1.0% RMS. Figure 1 is a schematic diagram of the two-dimensional rectangular cavity model, which is formed by three 10mm thick Perspex plates. The model dimensions are as follows; cavity length, L = 100mm, cavity depth, D = 20mm and the model span, W is equivalent to the width of the water tunnel which is 380mm. The length-to-depth ratio, L/D = 5 and the span-to-depth ratio, W/D = 19, thus the flow can be considered nominally two-dimensional.

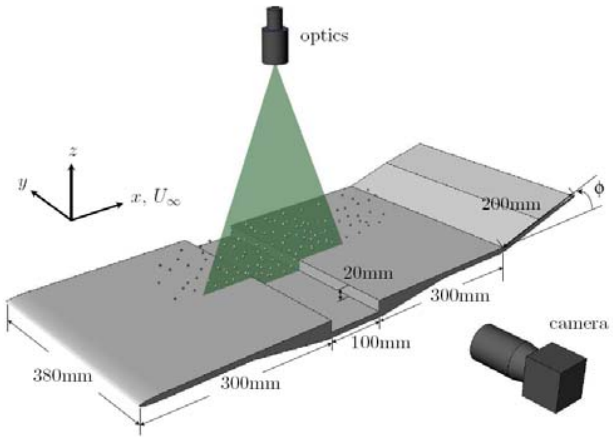

Figure 1. Cavity model dimensions and PIV experimental setup.

The front plate leading edge comprises of a modified super elliptical profile (with aspect ratio 6:1 and exponent n=3) as recommended by [8]. Due to the geometric asymmetry between the regions above and below the flat plate, a deflection plate was required downstream of the cavity in order to adjust the circulation around the model and obtain the stagnation point on the leading edge tip. For all the flow velocities tested the deflection plate was set at an angle of ϕ =15° from the horizontal plane, as shown in Figure 1. Flow visualisation and PIV measurements confirmed that with this arrangement the flow approaches parallel to the leading edge and develops along the upstream plate without separation.

The range of Reynolds numbers tested in this study allowed the onset of cavity shear layer oscillations and the transition to turbulence to be investigated. In Table 1, the flow velocities tested and the corresponding Reynolds numbers, Re_{300mm}, Re_δ and Re_D are presented. These Reynolds numbers are based upon a development length of 300mm, the boundary layer thickness (δ) at the upstream edge of the cavity for a laminar Blasius boundary layer (using a development length of 300mm), and the cavity depth D = 20mm, respectively.

U_∞ (*mm/s*)	50.1	97.2	190.8	288.2
Re_{300mm}	1.5 x 10^4	2.9 x 10^4	5.7 x 10^4	8.6 x 10^4
Re_δ	610	850	1190	1463
Re_D	990	1930	3780	5710
Δt (*ms*)	2.0	1.0	0.50	0.35

Table 1. Flow velocities tested and the corresponding Reynolds numbers based on different parameters. The pulse separation time (Δt) is also given.

PIV measurements of the upstream boundary layer were taken at 5mm from the cavity leading edge. The mean flow boundary layer profile for each Reynolds number is plotted in Figure 2, and were derived by averaging 100 instantaneous vector fields. The profiles are shown to compare well with a Blasius laminar profile.

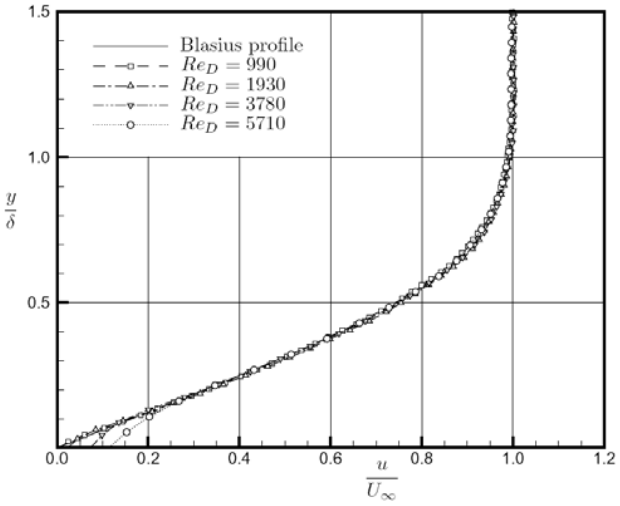

Figure 2. Boundary layer velocity profiles 5mm upstream of the cavity upstream face for the various Re_D tested.

Experimental Methodology

To visualise the free shear layer, fluorescent Sodium Fluorescein dye was injected through a 1.5 mm tube, located 3mm from the upstream face of the cavity via a constant pressure system.

In a steady flow the dye follows the pathlines to form streaklines from the point of injection. In an unsteady flow the streaklines do not necessarily coincide with instantaneous streamlines. The transport mechanism for dye (a passive scalar) and vorticity are different especially in regions of the flow where vortices are substantially stretched. Care must therefore be exercised when interpreting the flow visualisation dye patterns. The over-riding advantage of this method is that it can provide details of the large-scale nature of the flow.

For the PIV measurements, the 2D plane of interest was illuminated using a New Wave Solo PIV 200XT 532nm Nd:YAG laser, with 200mJ maximum pulse energy and a 5ns pulse width. The laser was mounted on an optical table which was levelled and positioned orthogonally to the cavity model. The laser generated the light sheet across the longitudinal centreline of the cavity model, as shown in Figure 1. The optical arrangement produced the desired sheet divergence to encompass the entire cavity and an appropriate laser sheet thickness for PIV measurements (measured to be 1mm at the cavity model surface).

The image acquisition system consisted of a TSI PowerView™ Plus 11 mega pixel CCD camera, fitted with a 105-mm Micro Nikkor f/2.8 lens. The CCD camera has a pixel resolution of 4008 x 2672, a pixel size of 9 x 9 μm and a frame rate of 2.07 Hz in frame straddling mode. The camera was mounted on a three degree of freedom translating system. Data acquisition and processing was achieved using the TSI INSIGHT™ 3G software with communication through the TSI LASERPULSE Synchronizer. The time intervals between laser pulses (Δt) are listed in Table 1, and they were based on a requirement that the maximum particle displacements be less than 25% of the 32×32 pixel Interrogation Window (IW).

The seed particles used were 30μm Potter's hollow glass spheres with a specific gravity (SG) of 0.34 ±0.02 and a particle relaxation time of ~17μs. The mass of seed particles added to the water tunnel was determined assuming a homogeneous distribution of particles and the presence of at least 8 particles in each IW. In PIV the assumption is made that the seed particles follow the local fluid velocity faithfully. Since the particles have a low SG, a small error may be introduced to the velocity measurement due to buoyancy. However, the maximum induced velocity due to buoyancy of the seed particles used in this experiment was estimated to be only $0.005U_\infty$. Taking a typical magnification case and a pulse separation time (Δt) of 2ms, the displacement of the seed particles due to buoyancy translates to 0.02 pixel. This buoyancy displacement is comparable with the displacement estimates of Soria [9] for 30μm and SG = 0.7 particles, and it is of the order of the resolution of the PIV measurement system.

For the image capture setup used, the particle image diameter was estimated to be 1.4 pixels. The systematic tendency of PIV measurements to bias towards integer pixel displacements is known as pixel-locking and can be assessed by plotting histograms of particle displacement. The global histograms plots for each case revealed an acceptable distribution thus indicating that pixel-locking was not evident in the current experiment.

The PIV data was taken for an image capture area of 6.36D x 4.24D and a spatial resolution of 32.03μm/pixel. The PIV data was processed through a two-pass recursive algorithm. The initial pass uses a 50% overlap grid spacing and an interrogation window (IW) of 62 x 62 pixels. The accuracy was improved and the spatial resolution is increased by reducing the IW to 32 x 32 pixels and offsetting the IW by the particle image displacement distance of the first processing pass. By offsetting the IW by the particle image displacement distance, lost pairs due to in-plane motion are effectively eliminated, thus increasing the signal-to-noise ratio. The resultant vector field was then passed through a validation and filtration process, which included a global velocity range filter, a median filter and a mean filter both using a neighbourhood size of 3x3 pixels and a tolerance of 0.5 pixels. Invalid data regions were interpolated and finally the data was smoothed using a Gaussian function with a neighbourhood size of 3x3 pixels and a Gaussian radius of 1.1.

Results and Discussion

Instantaneous flow field

Instantaneous flow visualisation images, separated by approximately a quarter of a shear layer shedding period (T) are shown in Figures 3 to 6 for each Re_D tested. The flow direction in Figures 3 to 6 and all subsequent figures is from left to right. The flow visualisation confirmed that the cavity flow was aerodynamically open for all the Reynolds numbers tested. Three distinct flow regimes were observed.

Regime I

The first regime was observed at Re_D = 990 and it was characterised by regular small amplitude oscillations of the shear layer and a slow moving steady recirculation region encompassing the entire cavity. The time sequence images in Figure 3 show this flow. A free shear layer emanates from the upstream face of the cavity and it is relatively unperturbed over the length of the cavity. A very small disturbance wave then propagates through the shear layer until it impinges on the downstream cavity face. At regular intervals, a portion of the shear layer is swept inside the cavity, as observed at t~T/4 and t~T/2. The swept-in portion of the dye moves downward along the vertical trailing wall. At t~3T/4, the disturbance wave is shed from the upper trailing edge of the cavity as the cycle begins again. Within the cavity, the fluid near the cavity floor is observed to curve over a recirculating bubble (which is evident in Figure 7) at approximately x/D = 0.65. Gradually, this fluid is stretched upstream by the large entrainment demands of the separated shear layer between the leading and trailing walls of the cavity. Overall, the flow pattern within the cavity appears to exhibit a large-scale clockwise recirculation region.

Regime II

Regular shear layer oscillations typify regime II. The flow in this regime is characterised by distinct, small amplitude disturbance waves within the separated shear layer. This regime is shown in Figure 4 and 5 at Re_D = 1930 and 3780, respectively. From Figure 4 and 5, disturbance waves are observed to periodically roll up and propagate downstream, appearing similar in size (amplitude) and structure. Partial clipping of disturbance waves is observed to occur on the downstream upper edge, resulting in a portion of the shear layer structure being shed downstream near the aft wall and the remainder being drawn into the cavity. Each such occurrence satisfies the entrainment demands of the shear layer at the upstream edge, resulting in a continuation of regular oscillations. For Re_D = 3780, the flow exhibits small periods of irregular oscillatory behaviour, typical of regime (III), and also an increased level of dye diffusion was evident within the cavity.

Regime III

The third regime occurred at Re_D = 5710 and contained irregular oscillatory behaviour. It was characterised by irregular 'flapping' of the shear layer and random shedding of varying amplitude disturbance waves. Figure 6 displays this behaviour as well as an increased diffusion of the dye within the cavity. Entire vortex structures are observed to alternately escape or be drawn completely into the cavity resulting in a large transfer of fluid into, and out of, the cavity. This large influx of fluid motion into the cavity causes the shear layer to oscillate with an irregular pattern. A return to more organised or regular shear layer oscillations (regime II) is observed when the fluid motion in the cavity begins to move in phase with the shear layer oscillations of the system.

At a particular Reynolds number, disturbances are observed to grow as they propagate downstream. As the Re_D is increased, the disturbance waves appear to be greater in amplitude. This behaviour is analogous to that of a free shear layer, as reported in [7]. Figures 3 to 6 also show that as the Reynolds number is increased, roll-up of the shear layer begins closer to the cavity upstream face, up to x/D = 0.5 at Re_D = 5710. This suggests a quicker transition of the shear layer to a turbulent state as the Re_D is increased. The variation of amplitude of the disturbances appears to be due to the selective amplification characteristics of the free shear layer flow and the additional feedback condition which is present because of the flow in the cavity.

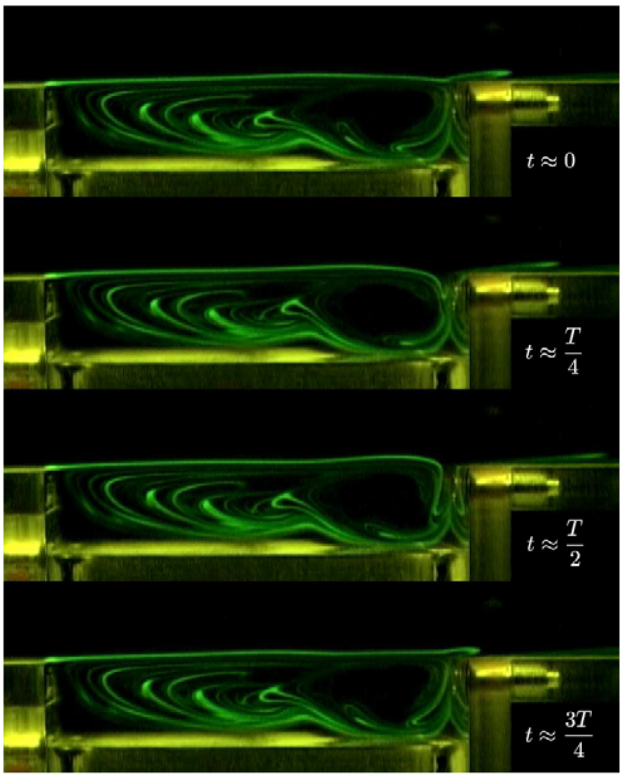

Figure 3. Regime I: Flow visualisation images at $Re_D = 990$; In this figure and subsequent flow visualisation images, the four panels show the flowfield at time instances separated by approximately a quarter of a shear layer shedding period cycle (T).

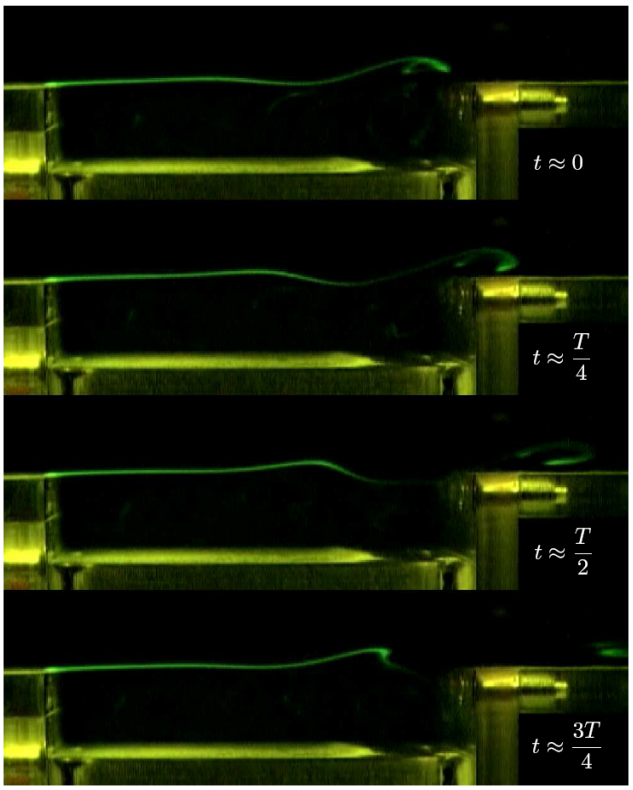

Figure 4. Regime II: Flow visualisation images at $Re_D = 1930$.

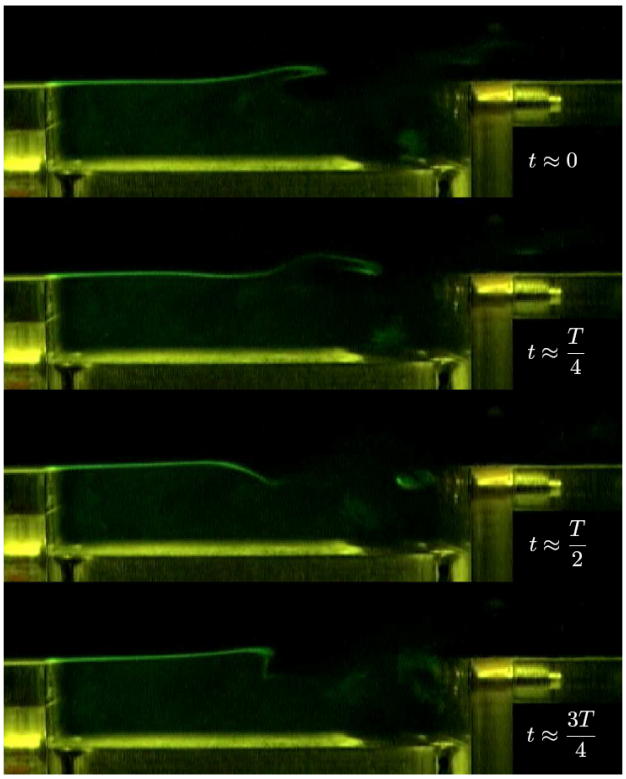

Figure 5. Regime II: Flow visualisation images at $Re_D = 3780$.

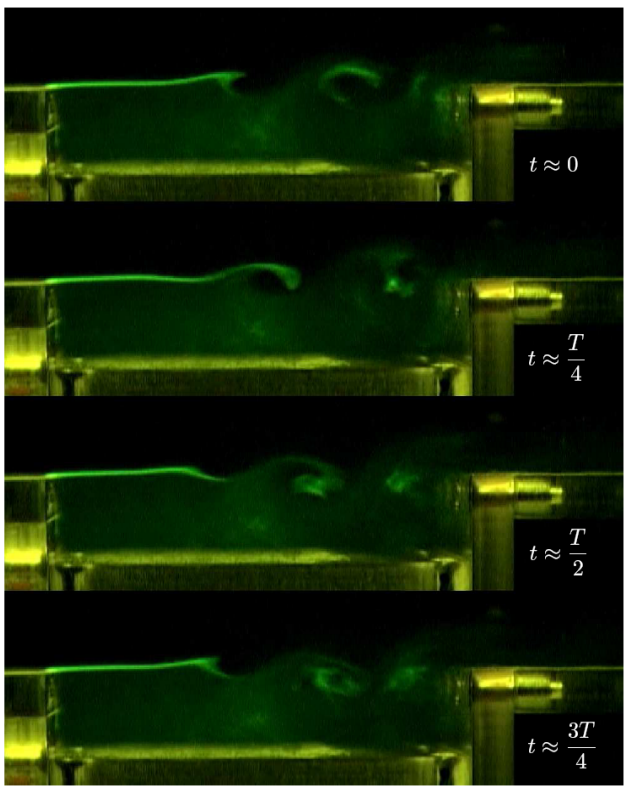

Figure 6. Regime III: Flow visualisation images at $Re_D = 5710$.

The flow regimes observed in this study are similar to those defined by Neary [4], but occur at higher Re_D. Neary [4] studied a cavity with L/D = 3.55 and did not investigate the effect of the cavity length on the three behaviours observed.

Mean flow fields

The mean PIV flow fields were obtained by averaging 250 instantaneous vector fields. A path integration of the mean velocity fields yields the topological streamline maps, presented in Figure 7 for the four Reynolds numbers tested. Figure 7 (a) shows that, for regime I, at Re_D = 990, a large-scale, clockwise recirculating mass of fluid encompasses most of the cavity with a separatrix streamline (node) dividing a pair of vortex cores. The entrainment of fluid from the cavity into the shear layer is evident from the streamline paths close to the upstream upper cavity edge. The fluid motion in this regime is fairly steady and a comparison between the flow visualisation and the PIV mean flow streamline topology reveals similar flow structures. The streamlines near the cavity floor are observed to curve over a small recirculation bubble as was evident in the flow visualisation (Figure 3).

Figure 7 (b) shows that at Re_D = 1930 (regime II) the streamline topology displays similar patterns, but in this case the recirculation bubble has increased in strength and it can be clearly seen as an anti-clockwise vortex on the cavity floor, located approximately at x/D = 0.65. A small anti-clockwise vortex is also present at the upstream cavity corner. As the Reynolds number is increased to 3780, (regime II) a similar overall pattern remains, however, in this case the large clockwise vortex at the downstream wall has increased in size and the smaller anti-clockwise vortex core appears to be stretched upstream.

In the third regime, at Re_D = 5710 which is shown in Figure 7 (d), a large clockwise recirculation structure dominates the majority of the cavity, and the upstream anticlockwise corner vortex has also broadened slightly. The mean flow patterns are generally in agreement with those observed in [3, 6] and they also display similarities with the data of [5] where the upstream boundary layer was turbulent.

Time-averaged out-of-plane vorticity

The time-averaged out-of-plane non-dimensional vorticity contours ($\omega_y D/U_\infty$) are presented in Figure 8. The shear layer appears as a concentrated region of negative vorticity that detaches from the upstream edge and diffuses with increasing distance downstream. As the downstream edge of the cavity is reached another concentration of negative vorticity is observed (but smaller in magnitude), which represents the clockwise recirculating corner vortex. Positive vorticity of significant magnitude is evident along the downstream cavity face and is observed to extend further upstream along the bottom wall of the cavity as the Re_D is increased. The concentrated region of negative vorticity in the shear layer is notably thicker as the Reynolds number is increased and is also pulled upstream, up to x/D = 0.6 at Re_D = 5710, as shown in Figure 8(d). This vorticity distribution in the shear layer indicates the unsteady nature and increased mixing evident in flow regimes II and III.

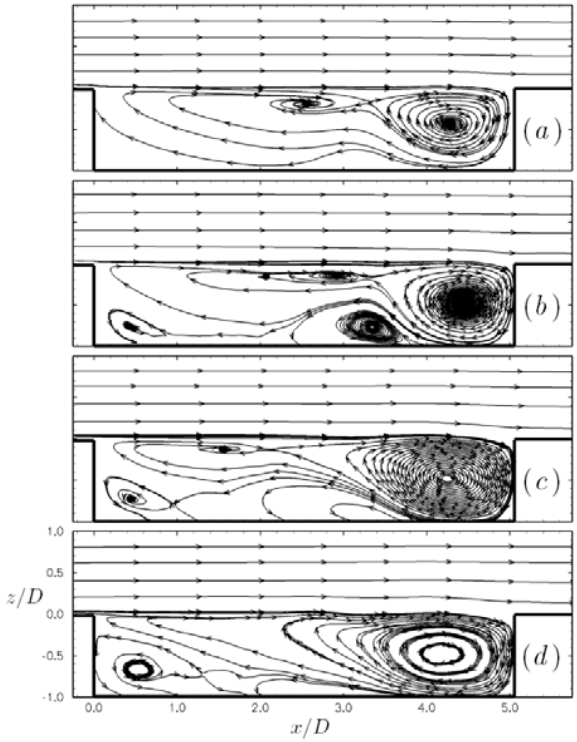

Figure 7. Time-averaged streamline topology: (a) Re_D = 990; (b) Re_D = 1930; (c) Re_D = 3780 and (d) Re_D = 5710.

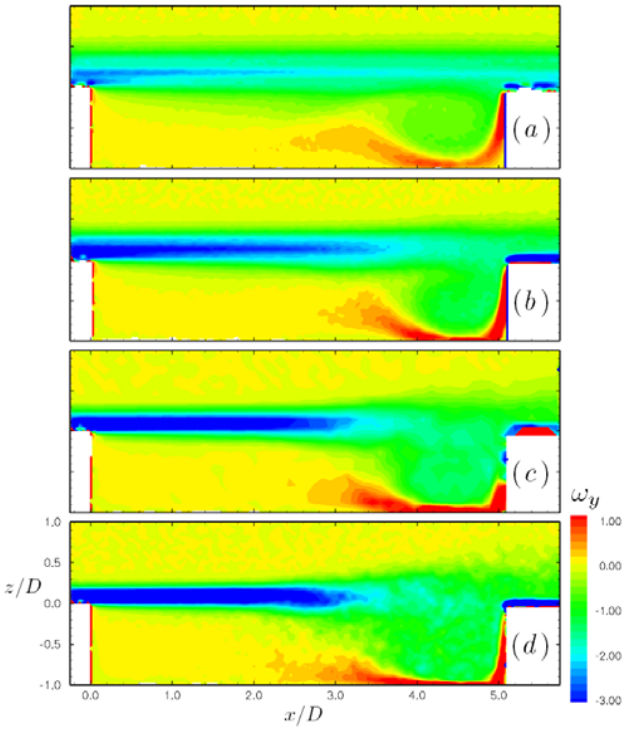

Figure 8. Time-averaged y-vorticity contours ($\omega_y D/U_\infty$): (a) Re_D = 990; (b) Re_D = 1930; (c) Re_D = 3780 and (d) Re_D = 5710.

Reynolds stress

The dimensionless Reynolds stress, $<u'v'>/U_\infty^2$ is presented in Figure 9. The Reynolds stress displays the level of mixing and turbulence present in the flow. Regions of concentrated levels broaden out towards the leading edge of the cavity as the Re_D is increased. The Reynolds number has some influence on the Reynolds stress maximum value, with a small increase in the Reynolds stress maximum observed from Re_D = 1930 to Re_D = 3780. Figures (9 to 11) (a) demonstrates the steady nature of the flow at Re_D = 990, in which no turbulence is evident in the entire cavity region.

Turbulence intensity

The u-component turbulence intensity is shown in Figure 10. As the Re_D is increased, broadening of concentrated regions towards the leading edge is observed. A significant portion of the concentrated region represents the primary vortex in the downstream corner. A smaller separated concentrated region, representing the secondary vortex, is also observed on the cavity floor in Figure 10(c). As the Re_D is increased to 5710, Figure 10(d), the primary vortex dominates the downstream cavity region and it merges with the secondary vortex on the floor.

The v-component turbulence intensity is shown in Figure 11. As the Re_D is increased, large magnitudes of v-component turbulence intensity are observed along the downstream vertical face of the cavity. This region is a result of the free shear layer flow impinging on the downstream upper corner and moving down over the cavity trailing face. The peak levels of v-component turbulence intensity in the trailing portion of the cavity enlarge towards the leading edge of the cavity but do not penetrate deep into the cavity as compared with the u-component. The Reynolds stress, u-component and v-component turbulence intensity plots display a flow structure and behaviour that is consistent with results published in [5] and [6].

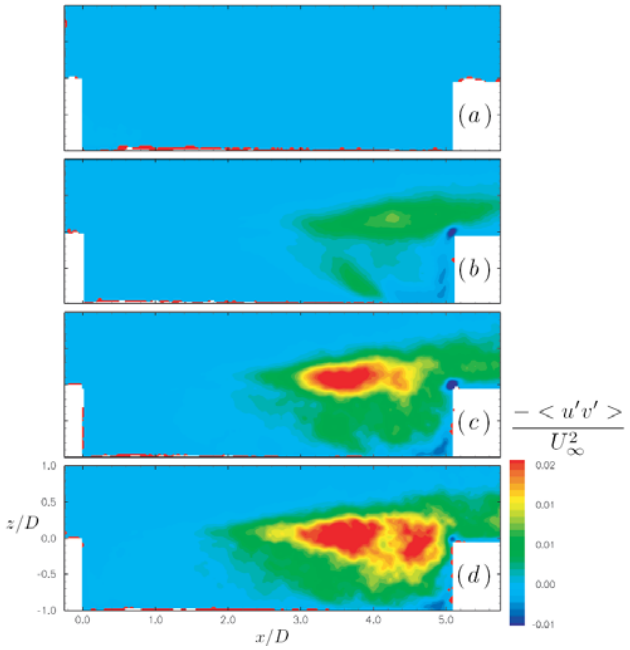

Figure 9. Reynolds stresses: (a) Re_D = 990; (b) Re_D = 1930; (c) Re_D = 3780 and (d) Re_D = 5710.

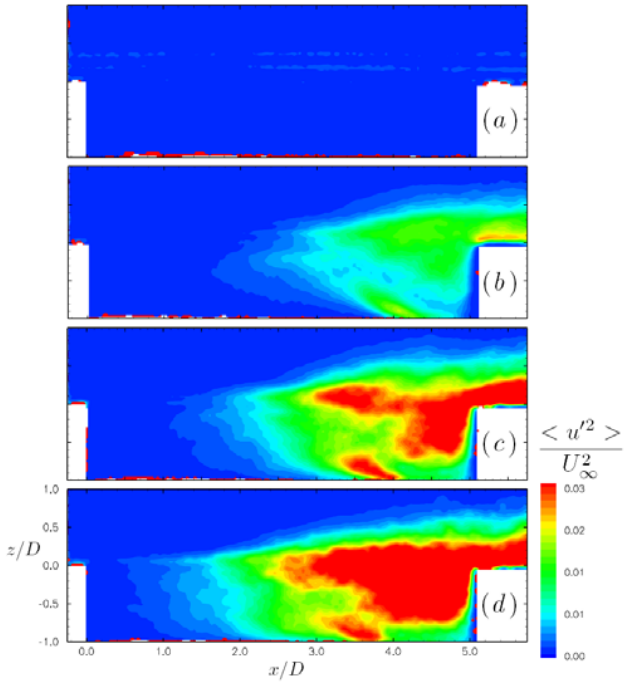

Figure 10. *u*-component turbulent intensity: (a) Re_D = 990; (b) Re_D = 1930; (c) Re_D = 3780 and (d) Re_D = 5710.

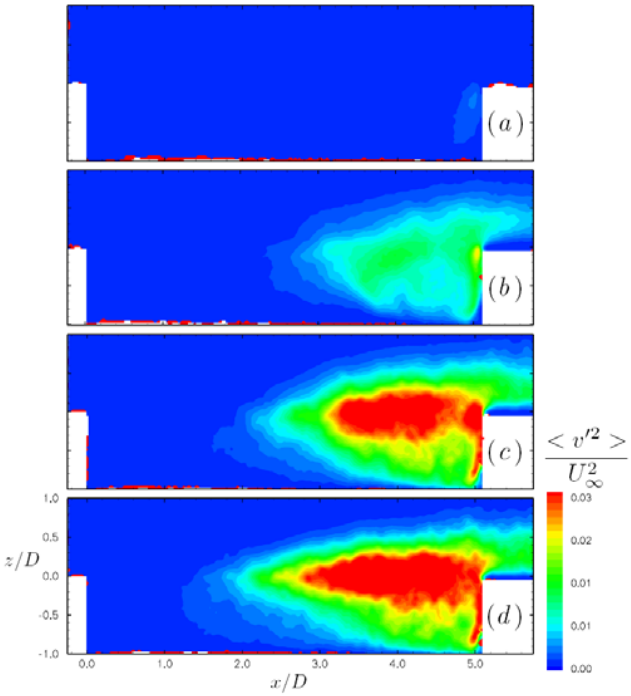

Figure 11. *v*-component turbulent intensity: (a) Re_D = 990; (b) Re_D = 1930; (c) Re_D = 3780 and (d) Re_D = 5710.

Conclusions

A preliminary assessment of the flow phenomena over a two-dimensional rectangular cavity has been made. Three flow regimes were identified using dye flow visualisation. Measurements using PIV showed the mean flow fields, in particular the streamline topology, to compare well with the flow visualisation images for the steady flow case at $Re_D = 990$. As the Re_D was increased the following features were noted; a primary vortex dominated the flow; the vorticity distribution in the shear layer indicated an increase in mixing and unsteadiness; and regions of maximum Reynolds stress, u-component and v-component turbulence intensity broadened towards the leading edge of the cavity. Results were found to compare well with existing PIV literature.

Acknowledgments

The author would like to thank Dr. Neil Matheson and Dr. Stephen Lam for providing assistance.

References

[1] Rossiter, J.E., Wind tunnel experiments on the flows over rectangular cavities at subsonic and transonic speeds, *Aeronautical Research Council Reports and Memoranda,* No. 3438, 1964.

[2] Sarohia, V., Experimental investigation of oscillations in flows over shallow cavities, *AIAA Journal,* **15 (7)**, 1977, 984-991.

[3] Grace, S.M., Dewar, G.W., Wroblewski, D.E., Experimental investigation of the flow characteristics within a shallow wall cavity for both laminar and turbulent upstream boundary layers, *Experiments in Fluids,* **36**, 2004, 791-804.

[4] Neary, M.D., Time-dependent Self-sustained Oscillations of Cavity Flow, AIAA *25th Aerospace Sciences Meeting*, Jan. 12-15, AIAA-87-10142, 1987.

[5] Rockwell, D., Lin, J.C., Organized oscillations of initially turbulent flow past a cavity, *AIAA Journal*, **39 (6)**, 2001, 1139-1151.

[6] Özsoy, E., Rambaud, P., Stitou, A., Riethmuller, M.L., Vortex characteristics in laminar cavity flow at very low Mach number, *Experiments in Fluids,* **38**, 2005, 133-145.

[7] Ashcroft, G., Zhang, X., Vortical structures over rectangular cavities at low speed, *Physics of Fluids,* **17**, 2005, 015104-015104-8.

[8] Narasimha R., Prasad S. N., Leading edge shape for flat plate boundary layer studies, *Experiments in Fluids,* **17**, 2004, 358-360.

[9] Soria, J., An investigation of the near wake of a circular cylinder using a video-based digital cross-correlation particle image velocimetry technique, *Experimental Thermal and Fluid Sciences*, **12**, 1996, 221-233.